THE JOURNAL OF PHYSICAL CHEMISTRY C

Feature Article

pubs.acs.org/JPCC

Electrodeposited Nanophotonics

Reginald M. Penner*,†,‡

†Department of Chemistry, University of California, Irvine, California 92697-2025, United States

‡Department of Chemical Engineering and Materials Science, University of California, Irvine, California 92697-2700, United States

ABSTRACT: Prior work involving the detection and emission of light from semiconductor nanostructures has involved single crystalline nanomaterials. Here we review the use of electrodeposited, polycrystalline (*pc*), cadmium selenide (CdSe) in nanowires and nanogap device structures for photonics. The photodetectors and photon emitters we describe are symmetrical metal−semiconductor−metal (M-S-M) devices prepared either by the evaporation of two gold contacts onto linear arrays of *pc*-CdSe nanowires prepared using lithographically patterned nanowires electrodeposition (*LPNE*), or by the electrodeposition of *pc*-CdSe directly onto gold nanogaps. The properties of these devices for detecting light using photoconductivity, and for generating light by electroluminescence, are described.

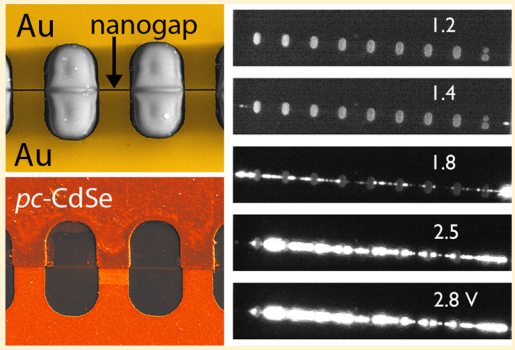

1. INTRODUCTION

The phrase "nanophotonics" pertains to the manipulation, detection, and emission of light to/from nanometer-scale devices.[e.g.1−18] Lieber et al. described the first light-emitting devices based upon semiconductor nanowires in 2001.[19,20] More recent work has explored the properties for light emission of single nanowires and arrays of nanowires,[21−24] core−shell heterostructures,[11,25−28] crossed nanowire p−n junctions,[8,17,29] and nanowire arrays interfaced to films.[30−34] Nanowire photoconductors for the detection of light were first demonstrated by Yang and co-workers using nanowires of both zinc oxide[35] and tin dioxide.[36] In addition to those two materials, subsequently studied by many,[37−44] other materials that were investigated included gallium nitride (GaN),[45−47] and cadmium sulfide (CdS).[48−51]

All of this prior research focused on devices that are based upon *single crystalline* semiconductor nanowires (for recent reviews, see refs:10,16,18,52,53). The case for employing single crystalline nanowires rather than polycrystalline nanowires in photonics devices is based upon prior work with both nanowires and films. If we consider photoconductivity, for example, the photocurrent, I_p is given by[54]

$$I_p = q\left(\eta\frac{P_{opt}}{h\nu}\right)\left(\frac{\mu\tau_{eff}\mathcal{E}}{L}\right) \quad (1)$$

where q is the elementary charge, P_{opt} is the incident optical power, η is the quantum yield, ν is the frequency of the incident light, μ is the carrier mobility, τ_{eff} is the effective minority carrier lifetime, $\mathcal{E}$ is the electric field (the applied voltage, V_{app}/L), and L is the distance between electrical contacts. Both μ and τ_{eff} are depressed by grain boundaries in polycrystalline semiconductor materials.[55,56] Polycrystalline nanowires[57−59] and films[60−65] have carrier mobilities that are a factor of $10-10^5$ lower than for single crystalline versions of the same material. Studies on silicon have shown that τ_{eff} is directly proportional to the mean grain diameter, across 5 orders of magnitude in both variables.[66] τ_{eff} is reduced significantly even in single crystalline silicon nanowires derived from the anisotropic etching of crystalline silicon wafers, highlighting the importance of carrier trapping and recombination at surface states.[67] Qualitatively, the same behavior is seen in compound semiconductor materials.[55,56] Although no data that we are aware of describes light emission from polycrystalline nanowires, researchers comparing single crystalline and polycrystalline films in light-emitting diodes have concluded that a reduction in the emission intensity by a factor of 100 is typical for polycrystalline films.[68]

In spite of the deficiencies outlined above, there are two motivations for investigating polycrystalline (*pc*) nanomaterials for photonics. The first is speed. τ_{eff} approximates the photocurrent decay time in the dark:[69,54,70]

$$I_p(t) = I_{p,0}\exp\left(\frac{-t}{\tau_{eff}}\right) \quad (2)$$

where $I_{p,0}$ is the dark current at a particular applied bias. The 3 dB bandwidth of the photoconductor, f_{3dB}, is inversely proportional to τ_{eff}:[70]

$$f_{3dB} = \frac{1}{2\pi\tau_{eff}} \quad (3)$$

Equation 3 predicts that the low values of τ_{eff} that are characteristic of polycrystalline materials correlates with a more rapid photoconductivity response and recovery. Commensurate with this expectation, fast (microsecond to picosecond) photoconductors based upon *pc*-CdSe and *pc*-CdTe films have been reported.[71−73] The response and recovery times for photoconductivity in these microscopic films are considerably faster

Received: April 15, 2014
Revised: June 2, 2014
Published: June 3, 2014

   dx.doi.org/10.1021/jp5037074 | *J. Phys. Chem. C* 2014, 118, 17179−17192

Table 1. Summary of Cadmium Chalcogenide-Based Photodetector Performance

absorber[a]	τ_{resp}: τ_{rec} [b]	photosensitivity S[c]	absorber and gap dimensions[d]	ref
CdSe film	1.0 ms: 1.5 ms	$10-10^8$	40 μm(gap) × 2.2 mm(w) × 700 nm(h)	136
CdSe film	1.6 ms: 1.6 ms	11	0.5 cm(gap) × 2.0 cm(w) × 750 nm(h)	137
CdSe film	1.0 ms: 0.2 ms	10^6	35 μm(gap) × 10 μm(w) × 300 nm(h)	72
CdSe film	1.3 ms: 0.2 ms	n.r.	1 cm^2(A) × 300 nm(h)	73
CdSe film	200 ms: 200 ms	10^3-10^7	5 mm(gap) × 5 mm(w) × 170 nm(h)	138
CdS nw	~15 ms: ~15 ms	39	20 μm(gap) × 200 nm(dia.) array	100
CdS nr	1s: 3s	1.5×10^3	200 nm−5 μm(w) × ~40 nm(h)	139
CdS nr	200 ms: 500 ms	2	25 μm(gap) × 640 nm(w) × 50 nm(h)	50
CdS nr	746 μs: 794 μs	9.2×10^3	18 μm(gap) × 10−60 μm(w) × 2−40 nm(h)	105
CdS nr	551 μs: 1.09 ms	3.3×10^6	50 nm(gap) × 5−10 μm(w) × 65 nm(h)	81
CdS nr	137 μs: 379 μs	$\sim 10^7$	13 μm(gap) × 500 nm(w)	140
CdTe nr	>1 s: >3 s	10	2 μm(gap) × 300 nm(dia.) vertical array	141
CdSe QD	~ 10 μs	100−6000	n.r.	112
CdSe QD	<1.0 ns: 3.5 ns	n.r.	5 μm(gap)	142
CdSe/ZnS QD	~5 μs	n.r.	~100 nm(gap)	143
CdSe nr	15 μs: 31 μs	100	~2.5 μm(gap) × 2−4 μm × 50−100 nm	144
CdSe nr	1 s: 200 μs	15	1−2 μm(gap) × 350 or 70 nm(dia.)	101
CdSe nr	1.7 ms: 6.7 ms	n.a	5 μm(gap) × 5 μm(w) × 60 nm(h)	113
CdSe nw	700 ms: 700 ms	40	3 μm(gap) × 60 nm(dia.)	86
pc-CdSe on carbon SWNTs	9 ms: 3 ms	~2	~8 μm(gap) × 30−60 nm(dia.)	102
CdSe nr	15 μs: 27 μs	$10-5 \times 10^7$	2.5 μm(gap) × 973 nm(w) × 87 nm(h)	144
_pc_-CdSe nw	**20 μs: 30 μs**	**10−100**	**5 μm(gap) × 200 nm(w) × 60 nm(h) array**	96
_pc_-CdSe ng	**~ 10 μs: 10 μs**	**~500**	**5−20 nm(gap) × 1 μm(w)**	98

[a]Abbreviations: QD = quantum dot; nw = nanowire; nr = nanoribbon; ng = nanogap; n.r. = not reported. [b]Response and recovery times as reported by the authors. [c]Photosensitivity = $S = (I_{photo}-I_{dark})/I_{dark}$. [d](gap) indicates the electrically isolated wire, rod, or channel length, if specified.

than most single crystalline nanowires, nanorods, etc. (Table 1). It is reasonable to assume that reducing the carrier lifetime will simultaneously make possible more rapid modulation of the electroluminescence from these devices, but this has not yet been investigated.

The second motivation involves the "nanowire integration problem". Incorporating single crystalline nanowires into electrical circuits is not straightforward. Such nanowires are obtained as orientationally disordered powders either from solution phase synthetic methods, or as a consequence of the removal of oriented nanowires from a surface as in vapor−liquid−solid (VLS) growth.[e.g74−82] How are individual nanowires extracted from these powders and positioned within an electrical circuit with the attachment of electrical contacts? A desire to solve the nanowire integration problem has brought about the development of new and innovative methods including contact printing of nanowires,[83−86] stamping oriented nanowire arrays onto adhesive-coated dielectrics,[87] flow orientation and patterning of nanowire ensembles,[14,14] dipping,[88] and mechanical alignment.[89,90] Each of these processes provides a different strategy for positioning a nanowire within a prefabricated electrical circuit.

Instead of making the circuit first and "plugging" nanowires into it, an alternative is to synthesize polycrystalline nanowires first, in a predetermined position and orientation on a dielectric substrate, and then fabricate the circuit on top of them (Figure 1). Lithographically patterned nanowire electrodeposition or *LPNE*,[92−94] provides a means for doing this. *LPNE* can be used to pattern arrays of thousands of CdSe nanowires, on glass, and other dielectrics.[59,95,96] In this article, I describe recent work from our laboratory in which we probe the properties of *pc*-CdSe nanowires and nanostructures for the detection and electrically stimulated emission of light.[91,95−100]

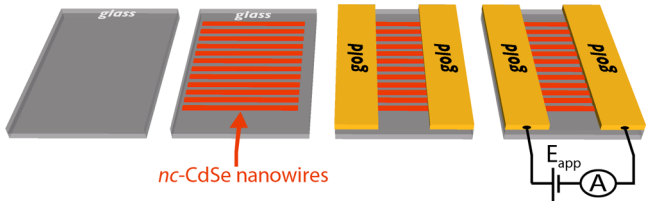

Figure 1. Schematic diagram depicting the fabrication of light-emitting M-S-M junctions starting with an array of *pc*-CdSe nanowires prepared using lithographically patterned nanowire electrodeposition (LPNE). Reprinted with permission of reference 91, copyright 2013, American Chemical Society.

Although polycrystalline nanomaterials have the potential to exhibit performance and device fabrication advantages relative to single crystalline materials, these advantages have been realized in few investigations to date. Mallouk and Keating et al.[101] were the first to study photoconductivity in *pc*-CdSe nanowires. In that work, gold−CdSe−gold segmented nanorods were prepared using template electrodeposition, and these structures showed a strong photoconductive response. Joselevich and co-workers[102] used carbon single-walled nanotubes to nucleate CdSe electrodeposition, forming *pc*-CdSe nanowires 134−174 nm in diameter. These structures showed rapid, sub-10 ms, response and recovery of their photoconductivity to light. We are aware of no other work in this area, aside from that of our own research group described below.

2. ELECTRODEPOSITION OF *pc*-CdSe NANOWIRES AND NANOGAP STRUCTURES

CdSe has been intensively studied for photonics applications. It is a direct band gap semiconductor with a band gap in the visible region of the spectrum (E_g = 1.75 eV, T = 298 K).

dx.doi.org/10.1021/jp5037074 | J. Phys. Chem. C 2014, 118, 17179−17192

Prior work includes applications of CdSe to field-effect transistors,[58,59,82,103−107] solar photovoltaics,[108−111] photodetectors,[95,96,112−114] and light-emitting diodes.[22,23,31] *pc*-CdSe nanowires were synthesized using the lithographically patterned nanowire electrodeposition or *LPNE* method (Figure 2a,b).[92−94]

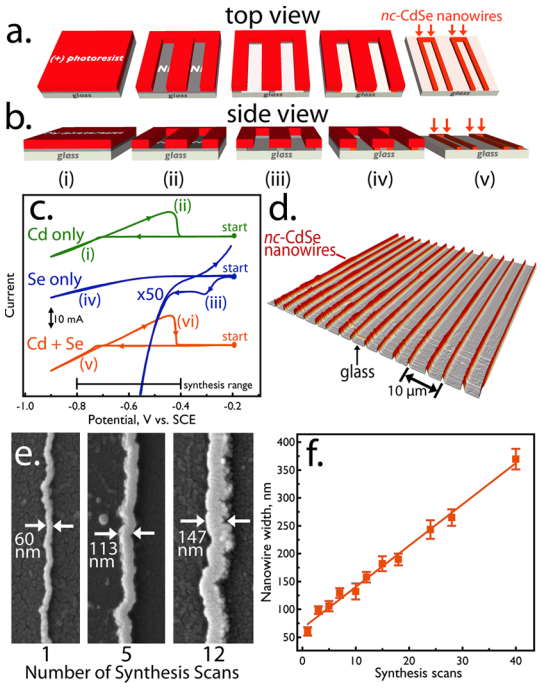

Figure 2. Synthesis of *pc*-CdSe nanowires: (a,b) Schematic diagram showing the five-step process flow for the synthesis by lithographically patterned nanowire electrodeposition (LPNE) of *pc*-CdSe nanowires - (i) a nickel layer and a (+)-photoresist (PR) layer are both deposited on a glass surface, (ii) the PR layer is patterned with a contact mask, (iii) nickel is etched from the patterned surface using nitric acid, (iv) *pc*-CdSe is electrodeposited from an aqueous solution containing both SeO_3^{2-} and Cd^{2+}. CdSe is deposited at the nickel electrodes - within the horizontal trench delineated on three sides by the PR, the glass surface, and the nickel electrodes. (v) PR and nickel are selectively removed to expose the *pc*-CdSe nanowires. (c) Cyclic voltammetry (50 mV/s) of plating solutions containing only Cd^{2+} (0.30 M, green), SeO_3^{2-} (0.70 mM, blue), and both precursors (orange). The electrolyte in all cases is 0.25 M H_2SO_4. The scan range used for the synthesis of *nc*-CdSe is indicated at bottom. (d) AFM image an array of *pc*-CdSe nanowires. (e) SEM images of single *pc*-CdSe nanowires prepared using 1, 5, and 12 synthesis scans. (f) Mean nanowire width versus the number of synthesis scans. Reprinted with permission of reference 95, copyright 2010, American Chemical Society.

The process flow for the *LPNE* synthesis of CdSe is as follows: A nickel layer is first evaporated on a glass surface, and photoresist is deposited onto the nickel surface (Figure 2a,b step (i)). The nickel layer thickness will dictate the thickness of the CdSe nanowire that is electrodeposited. This photoresist is then patterned using a contact mask (Figure 2a,b step (ii)), and the exposed nickel is removed by etching in nitric acid (Figure 2a,b (iii)). The etching time is adjusted during this process to "over etch" the nickel layer, producing an undercut around the entire perimeter of the exposed and developed region (Figure 2a,b (iii) - side view). This undercut forms a horizontal trench of width 500−800 nm. The height of this trench equals the thickness of the nickel layer. Next, a nanowire is electrodeposited within this trench using the nickel layer as a working electrode. Separate reference and counter electrodes, enabling potential control of the nickel edge, are also located in the electrochemical cell.

The most important step involves the electrodeposition of *pc*-CdSe nanowires (Figure 2a,b step (iv)). Near stoichiometric *pc*-CdSe nanowires[95,96,115,116] are obtained using the scanning electrodeposition/stripping method pioneered by Sailor et al.[117] Typical cyclic voltammograms (Figure 2c, orange trace) show a single, broad reduction wave that encompasses the formation of elemental cadmium and selenium and the formation of CdSe as the potential is scanned negatively from −0.20 V vs SCE to −0.90 V. On the ensuing positive scan, an oxidation wave signals the removal of excess cadmium from the nascent deposit. Elemental selenium is not removed within this potential window, and for this reason, a highly skewed Cd:Se molar ratio of 100:1, typically, is used in the plating solution to promote the conversion of selenium to CdSe instead of elemental selenium. By scanning the potential across this window multiple times, a *pc*-CdSe nanowire of the desired width is produced (e.g., Figure 2e,f).

The stoichiometry of the CdSe electrodeposit prepared using the electrodeposition/stripping procedure was investigated by X-ray photoelectron spectroscopy (XPS) and energy dispersive X-ray analysis (EDX) for CdSe nanowires prepared on graphite.[118] The molar ratio Se:Cd = 1.5−1.7 under the conditions shown in Figure 2c, but it is reduced to ∼1.1 if the nanowire is thermally annealed at 300 °C × 30 min in N_2.[118]

After electrodeposition of the CdSe, two modes for thermal processing can be applied to achieve the desired d_{ave} value (Figure 3): Heating the plating solution during the electro-

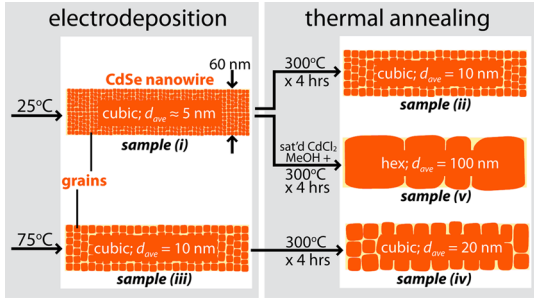

Figure 3. Schematic depiction of the influence of thermal processing on the mean grain diameter of *pc*-CdSe nanowires prepared using *LPNE*. Represented here is the cross section of nanowires with a height of 60 nm, taken perpendicular to the surface. Reprinted with permission of reference 96, copyright 2011, American Chemical Society.

deposition of CdSe, and thermal postprocessing of nanowires in an inert gas environment in an oven. The combination of these two processes provides the means for adjusting d_{ave} from 5 nm up to 100 nm for *pc*-CdSe nanowires, as shown schematically in Figure 3. The structure of the nanowires prepared by *LPNE* can be characterized using grazing incidence X-ray diffraction (GIXRD). GIXRD data are acquired using surfaces on which linear arrays of thousands of nanowires are deposited at an interwire pitch of 5 μm (e.g., Figure 2d). An estimate of the mean grain diameter, d_{ave}, is obtained from the GIXRD patterns using the line-width of the most intense (e.g., (111) for cubic CdSe) reflection according to the Scherrer eq:[119]

$$d_{ave} = 0.89\frac{\lambda}{B\cos\theta} \quad (4)$$

where d_{ave} is the mean grain diameter, λ is the X-ray wavelength, B is the full width of the peak measured at half-height, and θ is the diffraction angle. In typical GIXRD patterns of *pc*-CdSe

dx.doi.org/10.1021/jp5037074 | J. Phys. Chem. C 2014, 118, 17179−17192

nanowires deposited on glass surfaces (Figure 4a), the broad peak centered at 25° is contributed by diffuse reflection of X-rays from the amorphous glass surface. Narrower lines superimposed on this background are produced by reflections from CdSe. Two different crystal structures are achieved for the CdSe nanowires probed in Figure 4a: Trace (i) shows reflections for wurtzite phase CdSe nanowires while traces (ii–iii) all show patterns characteristic of cubic phase CdSe. The phase transition from cubic to wurtzite is induced by exposure of the CdSe nanowires to $CdCl_2$ in methanol prior to heating at 300 °C in N_2 for 4 h (Figure 5). Raman spectra, not shown here, provide information on the short-range structure of *pc*-CdSe nanowires that is also diagnostic of the crystallinity and the crystal structure.[91,98]

Electrodeposited *pc*-CdSe shows strong, band-edge photoluminescence at 1.75–1.80 eV (298 °C) and no perceptible trap state emission at lower energies. Neither the line width of this emission nor the peak energy is influenced significantly by the thermal processing described above.[95,96,98]

In the photonic devices constructed from these nanowires, the electrical contacts are separated by 0.5–5.0 μm, typically. Nanogap structures allow the influence of narrower spacings for the electrical contacts, making possible higher electrical fields, to be investigated. Thus, in addition to *pc*-CdSe nanowires, we have also prepared gold nanogap structures in which a nanometer-scale gap is formed in a gold film either by electromigration[98] or by focused ion beam (FIB) milling (Figure 6).[97] This gap, which can range in width from 5 nm in the case of electromigration[98] to 200 nm,[97] can then be bridged with electrodeposited *pc*-CdSe using the same electrodeposition procedure described in Figure 2c for nanowire growth (Figure 7).[97,98] The thermal annealing of gold nanogap structures is not possible, however, because of the instability of these nanogaps at the temperatures required for

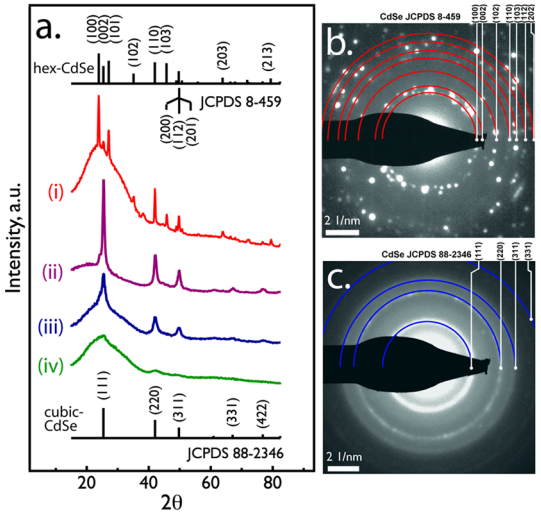

Figure 4. (a) Grazing incidence (incident angle = 0.3°) X-ray diffraction pattern (GIXRD) for arrays of *pc*-CdSe nanowires electrodeposited at 5 μm pitch on glass: (i) deposited at 25 °C, dipped in saturated $CdCl_2$:CH_3OH solution, and annealed (N_2, 300 °C, 4 h), (ii) deposited at 75 °C and annealed (N_2, 300 °C, 4 h), (iii) deposited at 75 °C; (iv) as-deposited at 25 °C. A broad reflection centered at ~25° in each pattern is derived from the amorphous glass surface. (b,c) Selected area electron diffraction patterns for (b) sample (i), and (c) sample (iii) showing the same principle reflections seen for these samples by XRD. The discontinuous diffraction rings seen in (b) are a consequence of the large grain dimensions in this sample. Reprinted with permission of reference 96, copyright 2011, American Chemical Society.

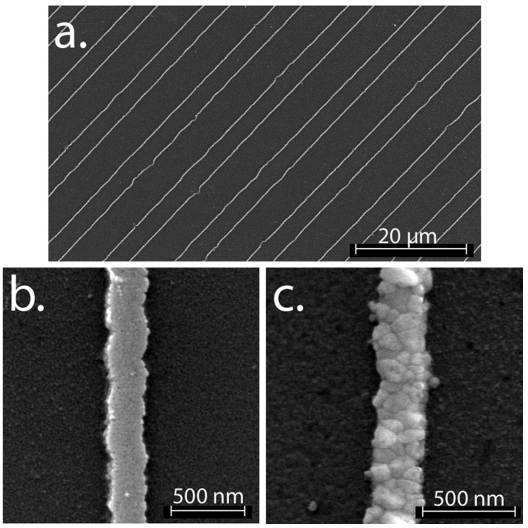

Figure 5. SEM images of: (a) an array of *pc*-CdSe nanowires and, at higher magnification, (b) *pc*-CdSe nanowires processed without, and, (c) with exposure to $CdCl_2$ in methanol. Reprinted with permission of reference 96, copyright 2011, American Chemical Society.

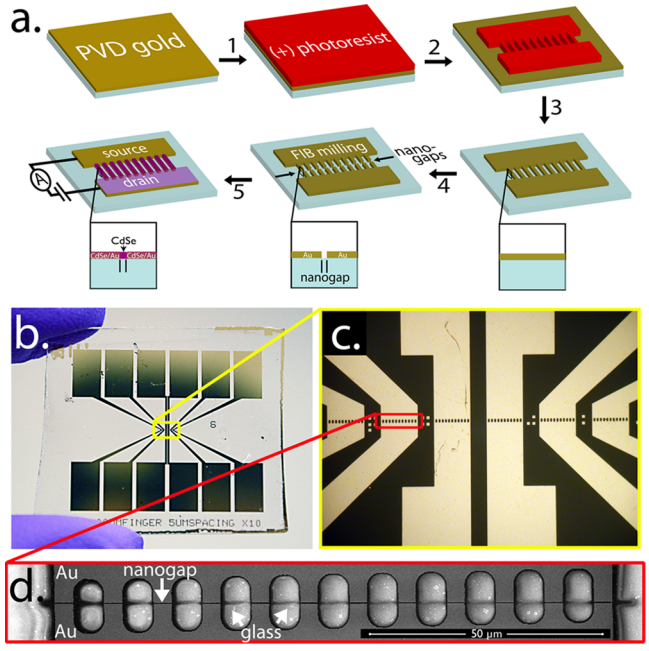

Figure 6. Fabrication of *pc*-CdSe filled, gold nanogap structures that function as light-emitting nanojunctions (LEnJs). (a) Schematic process flow for creating a nanogap and electrodeposition of *pc*-CdSe into it. (b) Photograph of a 2.5 cm × 2.5 cm glass slide showing six × twelve-nanogap arrays. (c) Optical micrograph of the six × twelve-nanogap arrays. (d) Scanning electron micrograph of a twelve-nanogap device characterized by 5 μm gold fingers after the fabrication by FIB of 200–250 nm nanogaps. Reprinted with permission of reference 97, copyright 2013, American Chemical Society.

CdSe grain growth.[97,98] It should be noted that the photonic properties of all devices were characterized in a laboratory air ambient (typically 20 °C and RH ≈ 55%). We did not systematically investigate the issue of stability, but device instability usually coincided with thermal damage caused by joule heating, sometimes culminating in the fracturing of the glass substrate on which the device was deposited. The use of substrates with higher thermal conductivities, such as crystalline silicon, might mitigate this issue.

dx.doi.org/10.1021/jp5037074 | *J. Phys. Chem. C* 2014, 118, 17179–17192

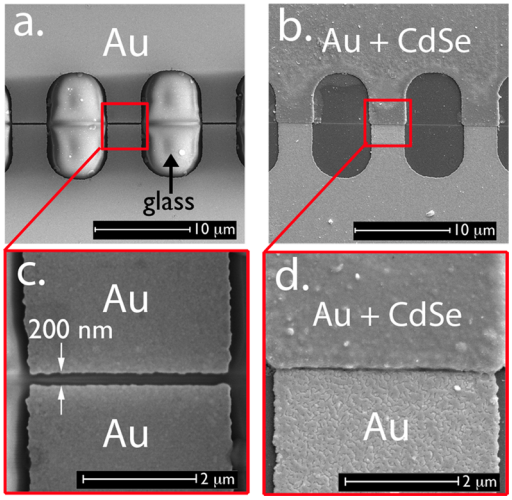

Figure 7. SEM images showing a gold nanogap prepared by FIB before and after electrodeposition of *pc*-CdSe. (a,b) Scanning electron micrographs of nanogaps formed by a single FIB milling (a) and same nanogaps after the electrodeposition of *pc*-CdSe (b). (c,d) Higher magnification images of the nanogap before (c) and after (d) *pc*-CdSe electrodeposition. Reprinted with permission of reference 97, copyright 2013, American Chemical Society.

3. PHOTODETECTORS BASED UPON PHOTOCONDUCTIVITY

Following the pioneering work of Mallouk and Keating et al.,[101] our research group began studying the photoconductivity of ensembles of *pc*-CdS wires in 2004.[100] Micro- and nanowires of CdS were obtained by first electrodepositing cadmium metal nanowires at the step edges present on a highly oriented pyrolytic graphite electrode, and then converting these cadmium nanowires to CdS by annealing in H_2S at 300°C for 30 min.[100] Ensembles of 10−100 *pc*-CdS nanowires prepared in this way were then transferred from the graphite surface to a dielectric, such as glass, and electrical contacts were prepared. This process, called electrochemical step edge decoration (*ESED*),[120−123] enabled the preparation of ensembles of very long (>1 mm) nanowires. After transfer to glass surfaces, ensembles of *pc*-CdS nanowires showed a strong photoconductivity response, characterized by a photosensitivity, $S = (I_{photo} - I_{dark})/I_{dark}$, of ∼40 and a rapid photoconductivity response with rise and recovery times in the 15 ms range—competitive with other II−VI nanowire-based photodetectors prepared up until that time.[100] Subsequently, stoichiometric *pc*-CdSe nanowires were prepared by *ESED* on graphite using an electrodeposition/stripping process that is similar to the process in use today (i.e., Figure 2c) but the photoconductivity response of those nanowires were not investigated.[99] However, the utility of *ESED* for device fabrication is limited both because of the requirement for nanowire transfer from the HOPG surface and because the arrangement of nanowires after transferring to a dielectric surface is dictated by the location of step edges on the graphite used for nanowire growth.

The deficiencies of the *ESED* process were addressed in 2006 by the development of a new process for electrochemical nanowire growth called lithographically patterned nanowire electrodeposition (*LPNE*).[92] As already described above (Figure 2a), *LPNE* provides a means for patterning nanowires prepared by electrodeposition directly on dielectric surfaces.[92−94] *LPNE* was applied to the synthesis of *pc*-CdSe nanowires in 2010.[95] Nanowires with lateral dimensions of 60 nm × 200 nm and millimeter scale lengths were prepared. These nanowires were close to stoichiometric and had a mean grain diameter of ∼10 nm. We found that arrays of 350 such nanowires showed a strong photoconductivity response with *S* in the range from 10 to 100 (Figure 8b), and response and recovery times of 20−40 μs

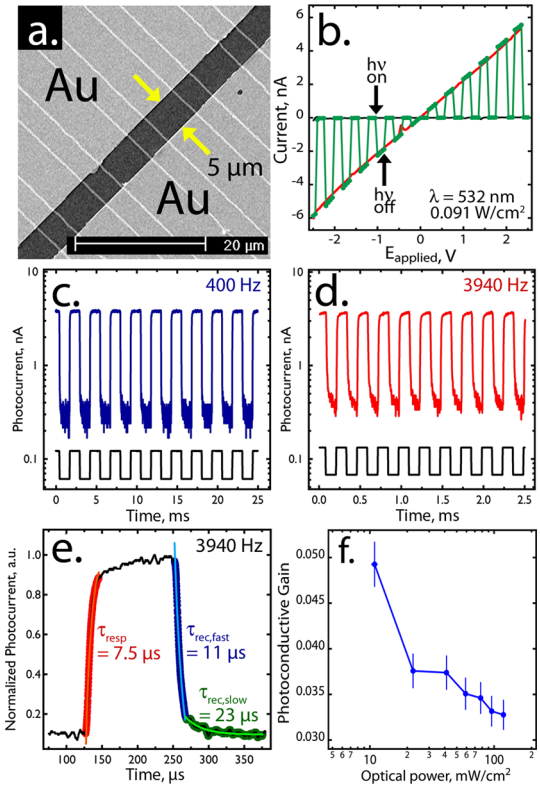

Figure 8. Characterization of *pc*-CdSe nanowires prepared by *LPNE*: (a) SEM images showing the 5 μm gap between evaporated gold electrodes. Nanowire arrays contained approximately 350 individual *pc*-CdSe nanowires. (b) Dark current (black) and photocurrent (red) versus applied bias for an array of 350 *pc*-CdSe nanowires. Also shown (green) is a current−voltage plot where the illumination (532 nm at 91 mW/cm²) was periodically interrupted to switch between the dark (black) and illuminated (red) curves. (c,d) Photocurrent response and recovery for arrays of 350 *pc*-CdSe nanowires. Modulation of the photocurrent as a function of time in response to chopped illumination (532 nm, 59 mW/cm²) at a frequency of: (c) 400 Hz, (d) 3940 Hz. Nanowires biased at 2 V. (e) Normalized photocurrent versus time showing three exponential fits and the associated time constants for the response (τ_{resp}) and recovery ($\tau_{rec,fast}$ and $\tau_{rec,slow}$) edges. (f) The photoconductive gain, $G = (I_{photo}/P_{optical})(h\nu/q)$ as a function of optical power. Reprinted with permission of reference 95, copyright 2010, American Chemical Society.

(Figure 8c−e)[95]—approximately 1/50th of the response and recovery times measured in the earlier work involving arrays of *pc*-CdS nanowires.[100] In addition to *S*, a second important metric for photoconductors is the photoconductive gain, *G*. *G*, the number of electrons measured by the device for each photon absorbed, is given by:[70]

$$G = \frac{\tau_{eff}}{\tau_{tr}} = \frac{\mu \tau_{eff} V}{l^2} \quad (5)$$

where τ_{tr} is the transit time for carriers between the two contacts, μ is the carrier mobility, *V* the applied voltage, and *l* is the

dx.doi.org/10.1021/jp5037074 | J. Phys. Chem. C 2014, 118, 17179−17192

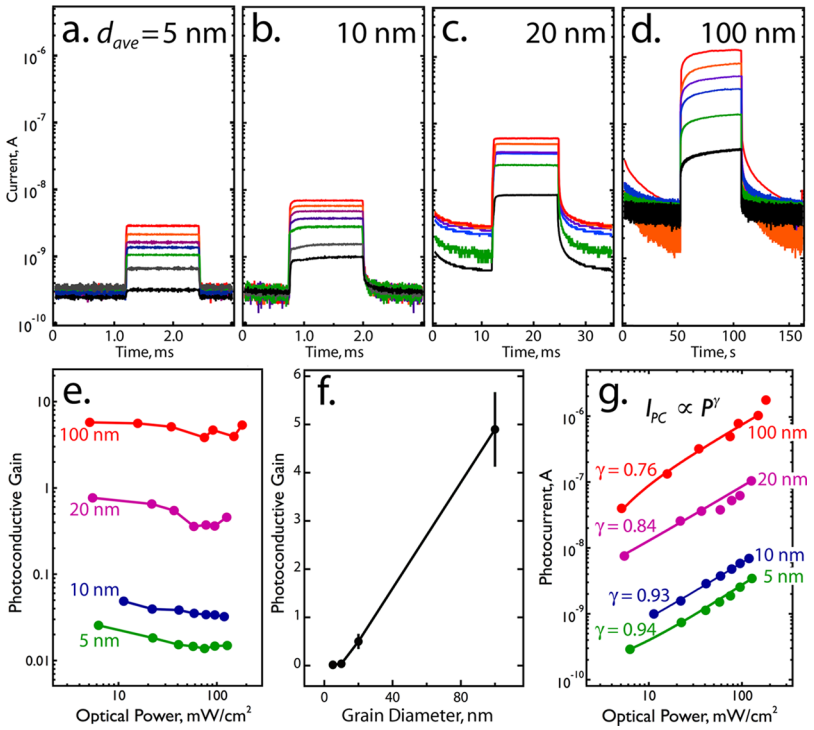

Figure 9. Influence of d_{ave} on the photoconductivity response of 350 *pc*-CdSe nanowire arrays: (a–d) Optical power-dependence of the photocurrent for four *nc*-CdSe nanowire arrays with d_{ave} as indicated. (e) Plot of *G* versus $P_{optical}$. (f) Plot of *G*, versus d_{ave}. (g) Correlation between the generated photocurrent and incident optical power of 350 *pc*-CdSe nanowires, plotted as the best fit to a simple power law: $i_{photo} \propto P^{\gamma}_{optical}$. Reprinted with permission of reference 96, copyright 2011, American Chemical Society.

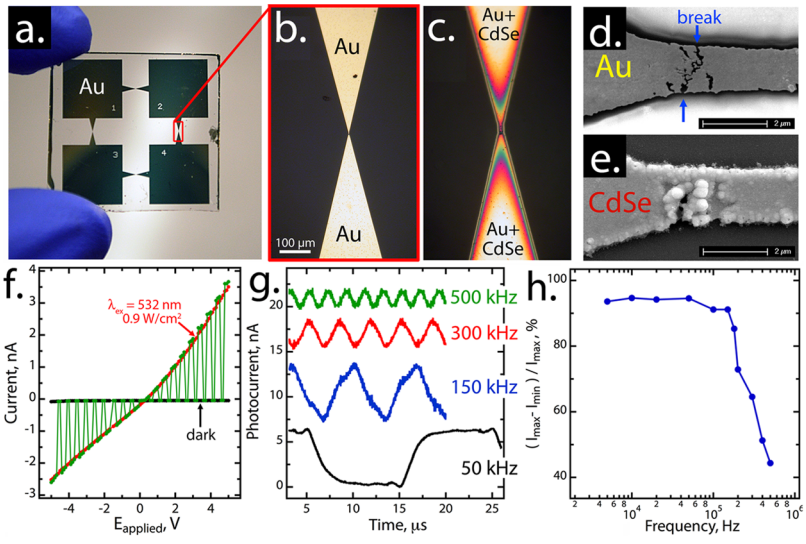

Figure 10. (a) Photograph of 1 in. × 1 in. glass slide with four Au bow-tie structures. (b) Optical micrograph of an individual bow-tie structure. (c) Same device after *pc*-CdSe deposition with the color change coming from the variation in thickness of *pc*-CdSe. (d,e) SEM images of a nanogap formed by feedback-controlled electromigration (d) and the same nanogap after the electrodeposition of *pc*-CdSe (e). (f) I_{dark} (black) and I_{photo} (red) versus applied bias for a Au–CdSe–Au nanogap photoconductor (λ_{ex} = 532 nm, 0.9 W/cm^2)). (g) Photocurrent versus time with illumination at 532 nm and 1.9 W/cm^2 modulated at frequencies of 50, 150, 300, 500 kHz. (h) Normalized photocurrent versus the modulation frequency. Reprinted with permission of reference 98, copyright 2012, American Chemical Society.

distance between contacts. In contrast to *p*–*n* or *p*–*i*–*n* photodiodes, photoconductor-based photodetectors are capable of producing *G* values that exceed one and can be as high as 10^6.[54] But *G* values measured for these nanocrystalline *pc*-CdSe nanowires were in the range from 0.032 to 0.050.[95] That is, the absorption of more than 20 photons was required to produce a signal of one electron in the measurement circuit.

Two strategies for increasing *G* were tested in subsequent studies: First, the mean grain diameter, d_{ave}, of the *pc*-CdSe nanowires was increased using thermal annealing coupled with hot electrodeposition, as already described above (Figures 3,4),[96] and second, the distance between the electrical contacts was dramatically reduced from the 5 μm value seen in Figure 8a by using gold nanogap structures having gap dimensions in the

dx.doi.org/10.1021/jp5037074 | *J. Phys. Chem. C* 2014, 118, 17179–17192

5−20 nm range.[98] The rationale for these two strategies is easily understood with reference to eq 5: Increasing the mean grain diameter was intended to increase τ_{eff}, which is proportional to G. The gap distance, on the other hand, is directly proportional to τ_{tr} and therefore inversely proportional to G.

Both of these approaches enhance G significantly. Increasing d_{ave} from 5 to 100 nm increases S from 8 to 300 and G by a factor of ∼30—from 0.02 to 6. However, the increase in d_{ave} caused an even stronger increase in the photocurrent response and recovery times, both of which increased by factors of 10^5−10^6 (see Figure 9). For example, the rise and recovery times for the d_{ave} = 10 nm nanowires are 8 μs, while that of d_{ave} = 100 nm nanowires are 8 s.[96] These data show very clearly that d_{ave} can be used to adjust the properties of *pc*-CdSe nanowires for detecting light, but the simultaneous optimization of bandwidth and gain is difficult. Increasing τ_{eff} increases both I_p (eq 1) and G (eq 5) but decreases f_{3db} (eq 3).

However, eq 5 also suggests a way to circumvent this catch-22: reduce l by employing nanogap structures instead of nanowires. Gold nanogaps with widths in the 5−20 nm range produced by electromigration (Figure 10a−d) were filled with electrodeposited *pc*-CdSe (Figure 10e) using the same procedure described in Figure 2.[98] The photoconductivity of these devices was characterized by a S = 500, $G \approx 45$, and response/recovery times (limited by our measurement circuit) of <2 μs, corresponding to f_{3db} > 175 kHz (Figure 10f−h)[98] Thus, nanogap structures allow a higher gain × bandwidth product to be accessed, allowing for the elevation of both G and f_{3db} simultaneously relative to the accessible G and f_{3db} for *pc*-CdSe nanowires.

The excellent photodetector performance obtained from *pc*-CdSe in both nanogaps and nanowires is surprising when it is considered that the grain boundaries present in *pc*-CdSe makes it a profoundly defective material that has, for example, low carrier mobilities, μ_{eff}, in the 10^{-4}−10^{-3} cm^2/(V s) range,[59] as compared with μ_{eff} = 650−800 cm^2/(V s) at 298 K for bulk CdSe.[54] However, these defects do not disqualify *pc*-CdSe for preparing efficient and fast photoconductive photodetectors. In fact, polycrystalline CdSe nanowires[95,96] and filled nanogaps[98] prepared by electrodeposition produce metrics for photodetection that rival or exceed those of single crystalline nanorods, nanowires, and nanoribbons (Table 1).

4. ELECTROLUMINESCENT NANOGAPS AND NANOWIRES

We are in the early stages of investigating the properties of electrodeposited *pc*-CdSe in symmetrical, metal−semiconductor−metal (M-S-M) junctions for generating light. The fabrication and evaluation of *pc*-CdSe-filled nanogap structures[97] and *pc*-CdSe nanowires[91] were both reported in 2013.

As already recounted above, the history of emissive nanowire devices dates to 2001.[19] Emissive nanogap structures[23,124−128] were first reported in 2002 by Dickson and co-workers[124−126] who observed electroluminescence (EL) from silver and gold nanoclusters located within metal nanogaps. Subsequently, light emission was seen from metal nanogaps containing single CdSe nanocrystals,[23] CdSe/ZnS (core/shell) nanocrystals,[128] and CdSe/ZnS (core/shell) nanocrystals.[127] The quantum efficiency, η, for light emission from M-S-M structures based upon cadmium chalcogenides, including nanogaps and nanowires is in the range from $\eta = 10^{-5}$ to 10^{-6}, while the threshold voltage for light emission, V_{th}, is 5−15 V.[22,23,128,129] However, all this prior work has involved investigations of single crystalline nanoparticles or nanowires, or ensembles of single crystalline nanostructures. Our initial goals in studying light emission from *pc*-CdSe was to understand whether this defective material could compete with single crystalline nanomaterials in terms of the critical light emission metrics.

Initial devices consisting of *pc*-CdSe-filled nanogap structures, referred to as light-emitting nanojunctions or *LEnJs*, are depicted in Figure 6.[97] Although gold nanogaps are not stable with respect to thermal annealing, *LEnJs* were prepared using two different electrodeposition temperatures, T_{dep}, = 20 °C and 75 °C in order to evaluate the influence of mean grain diameter (Figures 11,12).

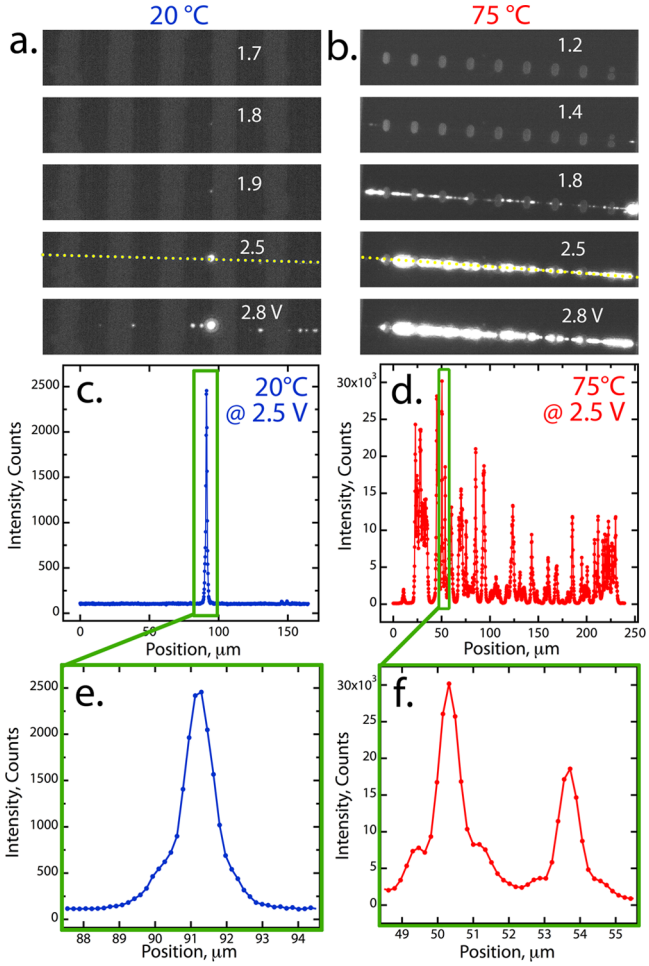

Figure 11. Optical micrographs and intensity profiles for *LEnJs*. (a,b) Optical micrographs showing EL as a function of the applied voltage (indicated in white). Data for T_{dep} = 20 °C (a) and 75 °C (b) are shown. All images were acquired using an integration time of 10 s. The dotted yellow line in the 2.5 V image coincides with the location of the nano gaps in these images. (c,d) Intensity profiles for 20 °C (c) vs 75 °C (d) along above dashed lines at 2.5 V. (e,f) Magnified traces of emission spots reveal that the full width at half-maximum intensity of each peak is ≤1 μm. Reprinted with permission of reference 97 copyright 2013, American Chemical Society.

Optical micrographs of *LEnJ* arrays (Figure 11a,b) show 10 *LEnJs* prepared using T_{dep} = 20 °C (a) or 75 °C (b). A subset of the *LEnJs* in each image begins emitting at an applied voltage, E_{app}, near 2 V, and the number of emitting junctions as well as the light intensity increases with E_{app}. Light emission is concentrated at ∼1 μm "hot spots" arrayed along the length of the 10 μm *LEnJs*. *LEnJs* prepared using T_{dep} = 75 °C have a higher probability for light emission as compared with devices prepared at 20 °C. Moreover, while the light emission process and current−voltage

dx.doi.org/10.1021/jp5037074 | J. Phys. Chem. C 2014, 118, 17179−17192

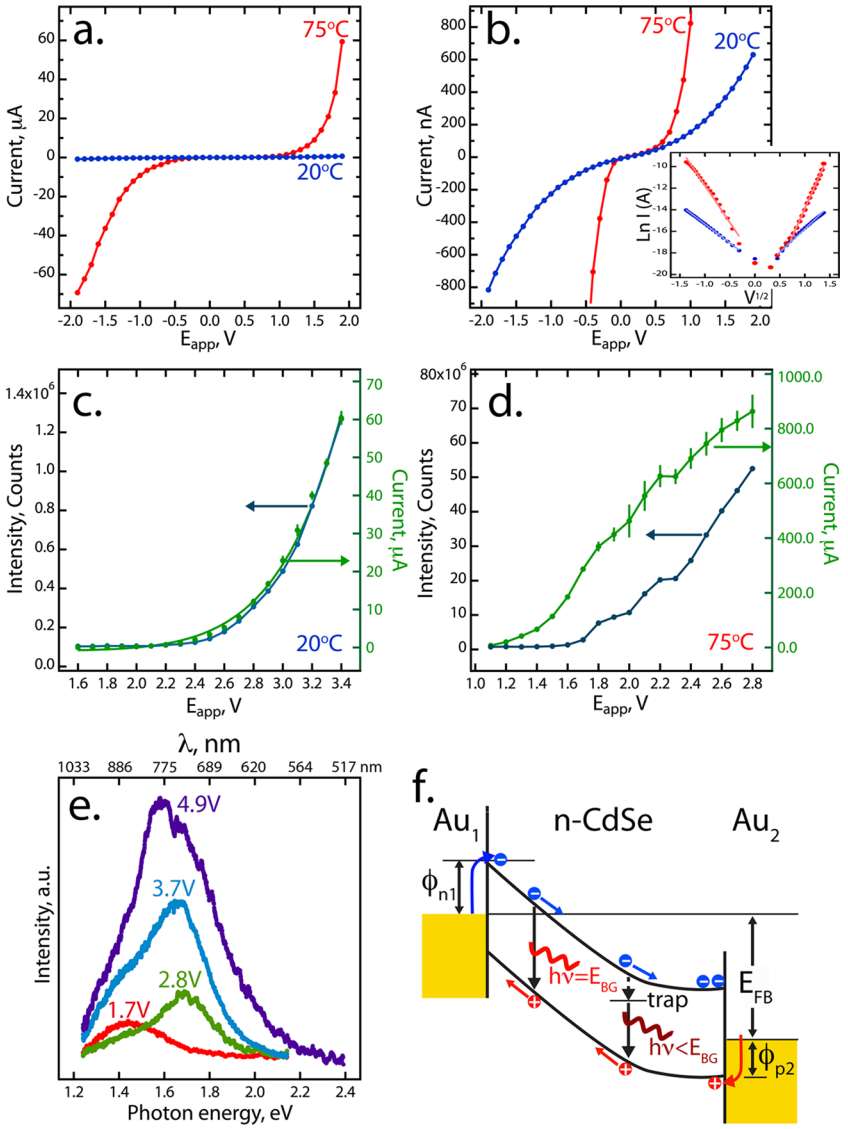

Figure 12. Electrical and optical characterization of *LEnJs*. (a) Current versus applied bias for Au−CdSe−Au nanogap devices fabricated at 20 °C (blue) vs 75 °C (red). (b) The same *I*−*V* data shown in (a) with rescaled current axes. Inset: Plot of ln *I* versus $V^{1/2}$ for these data showing the linearity of these plots. (c,d) EL intensity (left axis) and current (right axis) versus applied forward bias at 20 °C (c) vs 75 °C (d). e) EL emission spectrum for a typical *LEnJ* prepared from T_{dep} = 75 °C plating solution. (f) Energy level diagram depicting the M-S-M at an applied bias equal to the flat-band potential of the device, E_{FB} showing a reduction in the barrier for hole injection by V_{bi2}. Depicted here are two radiative recombination processes for electrons and holes responsible for the EL emitted by these devices. Reprinted with permission from reference 97, copyright 2013, American Chemical Society.

curves for these *LEnJs* are symmetrical with respect to the polarity of E_{app} (Figure 12a−d), the current and the light intensity measured at a particular E_{app} are both an order of magnitude higher for the 75 °C-deposited junctions. A preliminary conclusion is that light emission is promoted by the larger grain diameter of the *pc*-CdSe deposited at 75 °C (d_{ave} = 11 nm (75 °C) versus 6 nm (20 °C)).[97]

A spectrum of the emitted light for a *LEnJ* prepared using T_{dep} = 75 °C (Figure 12e) shows a broad emission envelope centered at 750 nm (~1.65 eV) at large values of E_{app} > 2.5 V, just below the 1.75 eV band gap of CdSe. However, a spectrum acquired at E_{app} = 1.7 V, near the threshold for light emission, is red-shifted to 890 nm (1.42 eV). This observation suggests that near the threshold voltage, light emission occurs from trapped electrons and holes, whereas for higher E_{app} and currents, near-band edge recombination occurs across the entire band gap of the *pc*-CdSe.[97]

Arrays of *pc*-CdSe nanowires (e.g., Figure 8a) behave similarly to *LEnJs* (Figure 13a−c).[91] Although EL emission from M-S-M junctions has been attributed to a variety of mechanisms,[23,54,130−132] several lines of evidence implicate Poole−Frenkel emission in the *LEnJs* and nanowire arrays described here.[91] Poole−Frenkel emission involves the electric field-driven "untrapping" of electrons and holes from defects; a prominent feature of our polycrystalline materials. Once liberated from traps, recombination and EL light emission from electrons and holes can occur. Both *LEnJs* (Figure 12b, inset) and nanowire arrays (Figure 13b) show a linear dependence of $Ln(I)$ on $E_{app}^{1/2}$ qualitatively as expected for Poole−Frenkel emission:[54,133,134]

$$I = I_0 \exp\left(\frac{\beta_{pf} V^{1/2}}{kTd^{1/2}}\right) \quad (6)$$

dx.doi.org/10.1021/jp5037074 | J. Phys. Chem. C 2014, 118, 17179−17192

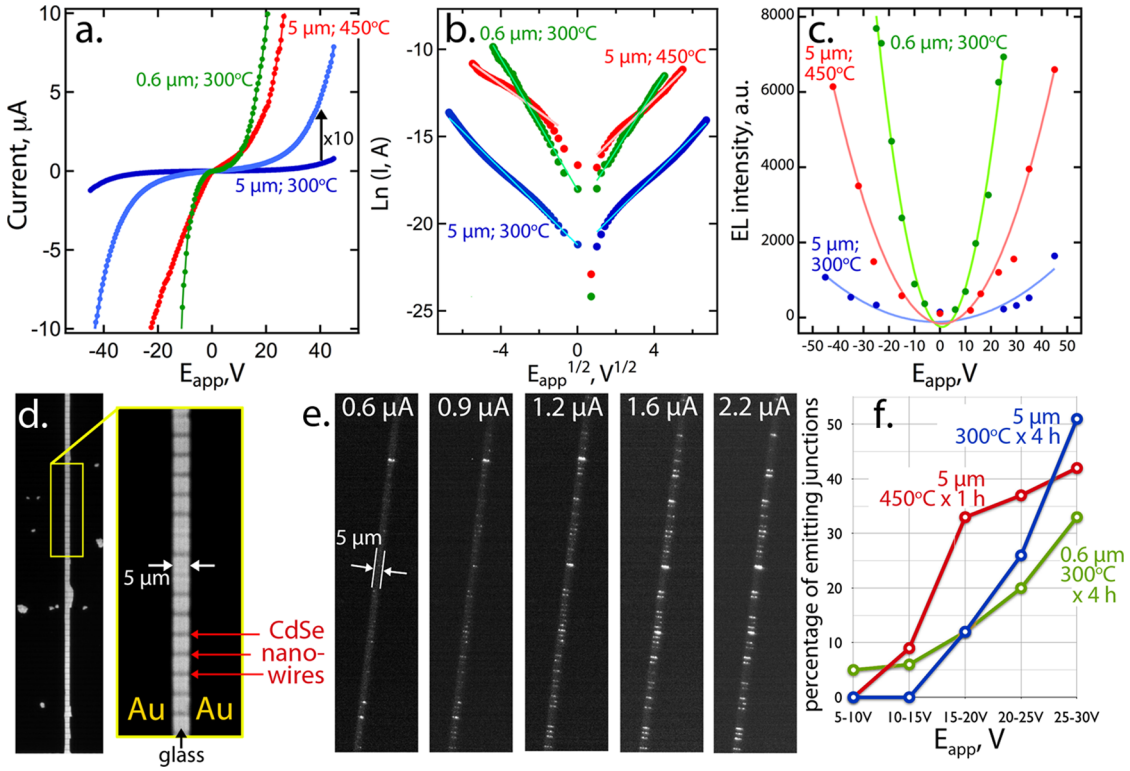

Figure 13. (a–c) Current versus voltage data (a,b) and EL intensity versus voltage (c) for three light-emitting junctions. (d) Brightfield optical micrograph of an *nc*-CdSe nanowire array. (e) Series of image of the EL emission for an array acquired at currents (E_{app}) of 0.6 μA (20 V), 0.9 μA (28 V), 1.2 μA (37 V), 1.6 μA (45 V), 2.2 μA (56 V). (f) Plot of the percentage of emissive nanowire junctions as a function of E_{app}. Reprinted with permission of reference 91, copyright 2013, American Chemical Society.

Table 2. Comparison of Device Metrics for Nanowire and Nanorod Light-Emitting Junctions and Diodes

emissive element[a]	device[b]	device length[c] (μm)	V_{th}[d] (V)	λ[e] (nm)	EQE[f]	ref
CdSe nr	M-S-M	0.030	1.75	750, 720	10^{-5}	23
CdSe nw	M-S-M	2–6	4	730	$(1–5) \times 10^{-6}$	22
CdSe nw + graphene	p–n	~2–3	4	705	n.r.	31
n-CdSe + p-Si nw	p–n	~1	n.a.	700	10^{-3}–10^{-2}	8
CdSe@ZnS nc's	M-S-M (M = Au)	0.1–0.2	1.60	680–820	n.r.	128
in ng	M-S-M (M = Pt/In)	0.1–0.2	~11	620–650	n.r.	128
CdSe@ZnS nc's	Si–S–Si	in STM	~17	500–750	n.r.	129
in STM						
n-InP + p-InP nw	p–n	~2	1.7	680, 820	10^{-5}	19
InP superlattice nw	p–n	10^{-3}	~1.0	n.r.	n.r.	145
GaN nw	n–i–n	n.a.	3	900	10^{-8}	21
p-GaN + n-Si nw	p–n	10^{-3}	6 (V_g = 2 V)	350–450	10^{-3}	8
GaN CMS nw	p–n	2–3	~4	tunable 380–650	0.039–0.058	11
***pc*-CdSe *LEnJs*:**						
T_{dep} = 20 °C	M-S-M	0.20	1.9 (±0.1)	780	$1.2(\pm0.4) \times 10^{-6}$	97
T_{dep} = 75 °C	M-S-M	0.20	1.5 (±0.2)	780	$1.8(\pm0.7) \times 10^{-6}$	97
***pc*-CdSe nw's:**						
300 °C × 4 h anneal	M-S-M	5	16 (±5)	n.r.	$6(\pm2) \times 10^{-7}$	91
450 °C × 1 h anneal	M-S-M	5	12 (±1)	n.r.	$8(\pm2) \times 10^{-7}$	91
300 °C × 4 h anneal	M-S-M	0.6	6.2 (±0.5)	750–780	$4(\pm1) \times 10^{-6}$	91

[a]Abbreviations: nc = nanocrystal, nr = nanorod, nw = nanowire, ng = nanogap. [b]Abbreviations: MSM = metal–semiconductor-metal, p-*n* = p–n junction photodiode. [c]The distance across the emissive element between the electrical contacts. [d]V_{th} = the threshold voltage for light emission. [e]λ = the wavelength range for light emission intensity. [f]EQE = external quantum efficiency.

where d is the thickness of the semiconductor layer, I_0 is the low-field current, and β_{pf} is the Poole–Frenkel field-lowering coefficient.[54,134] In the case of nanowires, EL light emission is concentrated in the vicinity of electrical contacts where the electrical fields, directly measured using scanning Kelvin probe microscopy, are also the highest.[91] While the contribution of

dx.doi.org/10.1021/jp5037074 | J. Phys. Chem. C 2014, 118, 17179–17192

other mechanisms for light emission can not be discounted, our data suggests that Poole−Frenkel emission is a prominent mechanism for EL in these systems.

As in the case of *LEnJs*, individual *pc*-CdSe nanowires progressively begin to emit light with increasing E_{app} (Figure 13d), contributing to EL intensities that increase quadratically with E_{app} (Figure 13c). Doh et al.[22] have reported similar intensity dependencies for single crystalline CdSe nanowires. This nanowire "turn on" process is documented by the photomicrographs (Figure 13e) showing part of a 350 nanowire device. Using data like that shown in Figure 13a and c, the external quantum efficiency (EQE) can be estimated[28,135]

$$\mathrm{EQE} = \frac{P_{opt}/h\nu}{I/e} \tag{7}$$

where P_{opt} is the measured optical power, h is Planck's constant, ν is the frequency of the emitted light, I is the current, and e is the elementary charge. For *pc*-CdSe nanowires[91] and *LEnJs*,[97] EQE values range from $(6-8) \times 10^{-7}$ to 1×10^{-6}. These values are certainly low, but they are virtually the same as EQEs measured for single crystalline CdSe nanowires[23] and nanorods[22] which produce values in the range from 10^{-5} to 10^{-6} (Table 2). In terms of maximizing the efficiency of light emission, tremendous opportunities exist for expanding our understanding and improving the performance of M-S-M devices based upon polycrystalline semiconductor materials.

5. SUMMARY

Electrodeposited polycrystalline CdSe is a versatile photonic material from which M-S-M devices can be obtained either by deposition into prefabricated metal nanogaps, or by nanowire formation using *LPNE*. These devices enable the detection of light by modulation of their photoconductivity, and the generation of light by electroluminescence. For the detection of light, the intrinsic defectiveness of *pc*-CdSe is actually an advantage, because it promotes rapid recombination of photoexcited carriers and a prompt return to the dark conductivity state from the photoconductive state of this material (eq 3). A bandwidth of up to 175 kHz has been measured for *LEnJs*[97] coupled with *S* up to 500—metrics that are competitive with the current state-of-the-art (Table 1). Surprisingly, the defects associated with grain boundaries do not handicap *pc*-CdSe relative to single crystalline CdSe for EL emission—EQE values are approximately the same for these systems. We speculate that *pc*-CdSe works reasonably well for EL because a channel for light emission, Poole−Frenkel emission, is facilitated in *pc*-CdSe relative to single crystalline CdSe, but more investigation will be required in order to understand and further optimize EL emission from polycrystalline semiconducting materials.

AUTHOR INFORMATION

Corresponding Author

*E-mail: rmpenner@uci.edu

Notes

The authors declare no competing financial interest.

Biography

Reginald Penner is Chancellor's Professor in the Departments of Chemistry and Chemical Engineering and Materials Science at the University of California, Irvine. He received B.A. degrees in Chemistry and Biology at Gustavus Adolphus College in Minnesota, and a Ph.D. at Chemistry at Texas A&M University working with Professor Charles R. Martin. After a postdoctoral appointment with Professor Nathan S. Lewis at Stanford and Caltech, he joined the faculty at UC Irvine in 1990. His research group studies the electrodeposition of nanomaterials, and the applications of these materials in devices including chemical sensors, biosensors, optical sensors and light emitters, batteries and capacitors.

ACKNOWLEDGMENTS

The work described here has been carried out by a corps of excellent, dedicated co-workers. Qiguang Li, Sheng-Chin Kung, Talin Ayvazian, and Wendong Xing were the lead scientists for the projects described here and are deserving of special recognition. The contributions of Dr. Wytze Van der Veer, Director of the Laser Spectroscopy Facility at UC Irvine Chemistry, were also invaluable in accomplishing this work. The author also gratefully acknowledges the financial support of this work by the National Science Foundation, Division of Chemistry and Division of Materials Research through contracts DMR-0654055, CHE-0956524, and DMR-1206867.

REFERENCES

(1) Barrelet, C. J.; Greytak, A. B.; Lieber, C. M. Nanowire Photonic Circuit Elements. *Nano Lett.* **2004**, *4*, 1981−1985.

(2) Barrelet, C. J.; Bao, J.; Loncar, M.; Park, H.-G.; Capasso, F.; Lieber, C. M. Hybrid Single-Nanowire Photonic Crystal and Microresonator Structures. *Nano Lett.* **2006**, *6*, 11−15.

(3) Claudon, J.; Bleuse, J.; Malik, N. S.; Bazin, M.; Jaffrennou, P.; Gregersen, N.; Sauvan, C.; Lalanne, P.; Gerard, J.-M. A Highly Efficient Single-Photon Source Based on a Quantum Dot in a Photonic Nanowire. *Nat. Photonics* **2010**, *4*, 174−177.

(4) Corcoran, B.; Monat, C.; Grillet, C.; Moss, D.; Eggleton, B.; White, T.; O'Faolain, L.; Krauss, T. Green Light Emission in Silicon Through Slow-Light Enhanced Third-Harmonic Generation in Photonic-Crystal Waveguides. *Nat. Photonics* **2009**, *3*, 206−210.

(5) Foster, M.; Gaeta, A.; Cao, Q.; Trebino, R. Soliton-Effect Compression of Supercontinuum to Few-Cycle Durations in Photonic Nanowires. *Opt. Express* **2005**, *13*, 6848−6855.

(6) Foster, M. A.; Turner, A. C.; Lipson, M.; Gaeta, A. L. Nonlinear Optics in Photonic Nanowires. *Opt. Express* **2008**, *16*, 1300−1320.

(7) Guo, X.; Qiu, M.; Bao, J.; Wiley, B. J.; Yang, Q.; Zhang, X.; Ma, Y.; Yu, H.; Tong, L. Direct Coupling of Plasmonic and Photonic Nanowires for Hybrid Nanophotonic Components and Circuits. *Nano Lett.* **2009**, *9*, 4515−4519.

(8) Huang, Y.; Duan, X.; Lieber, C. M. Nanowires for Integrated Multicolor Nanophotonics. *Small* **2005**, *1*, 142−147.
(9) Law, M.; Sirbuly, D. J.; Johnson, J. C.; Goldberger, J.; Saykally, R. J.; Yang, P. Nanoribbon Waveguides for Subwavelength Photonics Integration. *Science* **2004**, *305*, 1269−1273.
(10) Pauzauskie, P. J.; Yang, P. Nanowire Photonics. *Mater. Today* **2006**, *9*, 36−45.
(11) Qian, F.; Gradečak, S.; Li, Y.; Wen, C.-Y.; Lieber, C. M. Core/Multishell Nanowire Heterostructures as Multicolor, High-Efficiency Light-Emitting Diodes. *Nano Lett.* **2005**, *5*, 2287−2291.
(12) Sirbuly, D. J.; Law, M.; Yan, H.; Yang, P. Semiconductor Nanowires for Subwavelength Photonics Integration. *J. Phys. Chem. B* **2005**, *109*, 15190−15213.
(13) Tong, L.; Hu, L.; Zhang, J.; Qiu, J.; Yang, Q.; Lou, J.; Shen, Y.; He, J.; Ye, Z. Photonic Nanowires Directly Drawn from Bulk Glasses. *Opt. Express* **2006**, *14*, 82−87.
(14) Whang, D.; Jin, S.; Wu, Y.; Lieber, C. Large-Scale Hierarchical Organization of Nanowire Arrays for Integrated Nanosystems. *Nano Lett.* **2003**, *3*, 1255−1259.
(15) Yan, R.; Pausauskie, P.; Huang, J.; Yang, P. Direct Photonic-Plasmonic Coupling and Routing in Single Nanowires. *Proc. Natl. Acad. Sci. U.S.A.* **2009**, *106*, 21045−21050.
(16) Yan, R.; Gargas, D.; Yang, P. Nanowire Photonics. *Nat. Photonics* **2009**, *3*, 569−576.
(17) Zhong, Z.; Qian, F.; Wang, D.; Lieber, C. M. Synthesis of p-type Gallium Nitride Nanowires for Electronic and Photonic Nanodevices. *Nano Lett.* **2003**, *3*, 343−346.
(18) Zhai, T.; Li, L.; Wang, X.; Fang, X.; Bando, Y.; Golberg, D. Recent Developments in One-Dimensional Inorganic Nanostructures for Photodetectors. *Adv. Funct. Mater.* **2010**, *20*, 4233−4248.
(19) Duan, X.; Huang, Y.; Cui, Y.; Wang, J.; Lieber, C. Indium Phosphide Nanowires as Building Blocks for Nanoscale Electronic and Optoelectronic Devices. *Nature* **2001**, *409*, 66−69.
(20) Huang, M.; Mao, S.; Feick, H.; Yan, H.; Wu, Y.; Kind, H.; Weber, E.; Russo, R.; Yang, P. Room-Temperature Ultraviolet Nanowire Nanolasers. *Science* **2001**, *292*, 1897−1899.
(21) Zimmler, M. A.; Bao, J.; Shalish, I.; Yi, W.; Narayanamurti, V.; Capasso, F. A Two-Colour Heterojunction Unipolar Nanowire Light-Emitting Diode by Tunnel Injection. *Nanotechnol.* **2007**, *18*, 395201 (8 pp).
(22) Doh, Y.-J.; Maher, K. N.; Ouyang, L.; Yu, C. L.; Park, H.; Park, J. Electrically Driven Light Emission from Individual CdSe Nanowires. *Nano Lett.* **2008**, *8*, 4552−4556.
(23) Gudiksen, M.; Maher, K.; Ouyang, L.; Park, H. Electroluminescence from a Single-Nanocrystal Transistor. *Nano Lett.* **2005**, *5*, 2257−2261.
(24) Nguyen, H. P. T.; Djavid, M.; Cui, K.; Mi, Z. Temperature-Dependent Nonradiative Recombination Processes in GaN-based Nanowire White-Light-Emitting Diodes on Silicon. *Nanotechnol* **2012**, *23*, 194012 (6 pp).
(25) Tomioka, K.; Motohisa, J.; Hara, S.; Hiruma, K.; Fukui, T. GaAs/AlGaAs Core Multishell Nanowire-Based Light-Emitting Diodes on Si. *Nano Lett.* **2010**, *10*, 1639−1644.
(26) Hsu, W. C.; Chyan, J.-Y.; Lu, Y.-S.; Yeh, J. A. Electroluminescence of Out-of-Plane Silicon Nanowire/Silver Oxide/Silver Nanodendrite Heterostructures. *Opt. Mater. Express* **2011**, *1*, 1210−1215.
(27) Liu, C. Y.; Xu, H. Y.; Ma, J. G.; Li, X. H.; Zhang, X. T.; Liu, Y. C.; Mu, R. Electrically Pumped Near-Ultraviolet Lasing from ZnO/MgO Core/Shell Nanowires. *Appl. Phys. Lett.* **2011**, *99*, 063115 (3 pp).
(28) Bavencove, A.-L.; Tourbot, G.; Garcia, J.; Desieres, Y.; Gilet, P.; Levy, F.; Andre, B.; Gayral, B.; Daudin, B.; Dang, L. S. Submicrometre Resolved Optical Characterization of Green Nanowire-Based Light Emitting Diodes. *Nanotechnol.* **2011**, *22*, 345705 (9 pp).
(29) Kim, K.; Kang, J.; Lee, M.; Yoon, C.; Cho, K.; Kim, S. Ultraviolet Electroluminescence Emission from n-Type ZnO/p-Type Si Crossed Nanowire Light-Emitting Diodes. *Jpn. J. Appl. Phys.* **2010**, *49*, 06GG05.
(30) Bao, J.; Zimmler, M. A.; Capasso, F.; Wang, X.; Ren, Z. F. Broadband ZnO Single-Nanowire Light-Emitting Diode. *Nano Lett.* **2006**, *6*, 1719−1722.
(31) Ye, Y.; Gan, L.; Dai, L.; Meng, H.; Wei, F.; Dai, Y.; Shi, Z.; Yu, B.; Guo, X.; Qin, G. Multicolor Graphene Nanoribbon/Semiconductor Nanowire Heterojunction Light-Emitting Diodes. *J. Mater. Chem.* **2011**, *21*, 11760−11763.
(32) Hahn, C.; Zhang, Z.; Fu, A.; Wu, C. H.; Hwang, Y. J.; Gargas, D. J.; Yang, P. Epitaxial Growth of InGaN Nanowire Arrays for Light Emitting Diodes. *ACS Nano* **2011**, *5*, 3970−3976.
(33) Chen, C.-Y.; Zhu, G.; Hu, Y.; Yu, J.-W.; Song, J.; Cheng, K.-Y.; Peng, L.-H.; Chou, L.-J.; Wang, Z. L. Gallium Nitride Nanowire Based Nanogenerators and Light-Emitting Diodes. *ACS Nano* **2012**, *6*, 5687−5692.
(34) Zimmler, M. A.; Voss, T.; Ronning, C.; Capasso, F. Exciton-Related Electroluminescence from ZnO Nanowire Light-Emitting Diodes. *Appl. Phys. Lett.* **2009**, *94*, 241120 (3 pp).
(35) Kind, H.; Yan, H.; Messer, B.; Law, M.; Yang, P. Nanowire Ultraviolet Photodetectors and Optical Switches. *Adv. Mater.* **2002**, *14*, 158−160.
(36) Law, M.; Kind, H.; Messer, B.; Kim, F.; Yang, P. Photochemical Sensing of NO_2 with SnO_2 Nanoribbon Nanosensors at Room Temperature. *Angew. Chem., Int. Ed.* **2002**, *41*, 2405−2408.
(37) Fan, Z.; Chang, P. C.; Lu, J. G.; Walter, E. C.; Penner, R. M.; Lin, C. H.; Lee, H. P. Photoluminescence and Polarized Photodetection of Single ZnO Nanowires. *Appl. Phys. Lett.* **2004**, *85*, 6128−6130.
(38) Zhou, J.; Gu, Y.; Hu, Y.; Mai, W.; Yeh, P.-H.; Bao, G.; Sood, A. K.; Polla, D. L.; Wang, Z. L. Gigantic Enhancement in Response and Reset Time of ZnO UV Nanosensor by Utilizing Schottky Contact and Surface Functionalization. *Appl. Phys. Lett.* **2009**, *94*, 191103 (3pp).
(39) Ahn, S.-E.; Ji, H. J.; Kim, K.; Kim, G. T.; Bae, C. H.; Park, S. M.; Kim, Y.-K.; Ha, J. S. Origin of the Slow Photoresponse in an Individual Sol-Gel Synthesized ZnO Nanowire. *Appl. Phys. Lett.* **2007**, *90*, 153106 (3pp).
(40) Soci, C.; Zhang, A.; Xiang, B.; Dayeh, S. A.; Aplin, D.; Park, J.; Bao, X.; Lo, Y.-H.; Wang, D.; ZnO Nanowire, U. V. Photodetectors with High Internal Gain. *Nano Lett.* **2007**, *7*, 1003−1009.
(41) He, J. H.; Chang, P. H.; Chen, C. Y.; Tsai, K. T. Electrical and Optoelectronic Characterization of a ZnO Nanowire Contacted by Focused-Ion-Beam-Deposited Pt. *Nanotechnol.* **2009**, *20*, 135701 (5pp).
(42) Prades, J. D.; Jimenez-Diaz, R.; Hernandez-Ramirez, F.; Fernandez-Romero, L.; Andreu, T.; Cirera, A.; Romano-Rodriguez, A.; Cornet, A.; Morante, J. R.; Barth, S.; et al. Toward a Systematic Understanding of Photodetectors Based on Individual Metal Oxide Nanowires. *J. Phys. Chem. C* **2008**, *112*, 14639−14644.
(43) Li, Y.; Valle, F. D.; Simonnet, M.; Yamada, I.; Delaunay, J.-J.; High-Performance, U. V. Detector Made of Ultra-Long ZnO Bridging Nanowires. *Nanotechnol.* **2009**, *20*, 045501 (5pp).
(44) Keem, K.; Kim, H.; Kim, G.-T.; Lee, J. S.; Min, B.; Cho, K.; Sung, M.-Y.; Kim, S. Photocurrent in ZnO Nanowires Grown From Au Electrodes. *Appl. Phys. Lett.* **2004**, *84*, 4376−4378.
(45) Calarco, R.; Marso, M.; Richter, T.; Aykanat, A. I.; Meijers, R.; v.d. Hart, A.; Stoica, T.; Luth, H. Size-Dependent Photoconductivity in MBE-Grown GaN-Nanowires. *Nano Lett.* **2005**, *5*, 981−984.
(46) Kang, M.; Lee, J.-S.; Sim, S.-K.; Kim, H.; Min, B.; Cho, K.; Kim, G.-T.; Sung, M.-Y.; Kim, S.; Han, H. S. Photocurrent and Photoluminescence Characteristics of Networked GaN Nanowires. *Jpn. J. Appl. Phys.* **2004**, *43*, 6868−6872.
(47) Han, S.; Jin, W.; Zhang, D.; Tang, T.; Li, C.; Liu, X.; Liu, Z.; Lei, B.; Zhou, C. Photoconduction Studies on GaN Nanowire Transistors Under UV and Polarized UV Illumination. *Chem. Phys. Lett.* **2004**, *389*, 176−180.
(48) Jie, J. S.; Zhang, W. J.; Jiang, Y.; Meng, X. M.; Li, Y. Q.; Lee, S. T. Photoconductive Characteristics of Single-Crystal CdS Nanoribbons. *Nano Lett.* **2006**, *6*, 1887−1892.
(49) Ghosh, R.; Mallik, B.; Basak, D. Dependence of Photoconductivity on the Crystallite Orientations and Porosity of Polycrystalline ZnO Films. *Appl. Phys. A* **2005**, *81*, 1281−1284.
(50) Chen, J.; Xue, K.; An, J.; Tsang, S.; Ke, N.; Xu, J.; Li, Q.; Wang, C. Photoelectric Effect and Transport Properties of a Single CdS Nanoribbon. *Ultramicroscopy* **2005**, *105*, 275−280. Proceedings of the

Sixth International Conference on Scanning Probe Microscopy, Sensors and Nanostructures.
(51) Paul, G. S.; Agarwal, P. Persistent Photocurrent and Decay Studies in CdS Nanorods Thin Films. *J. Appl. Phys.* **2009**, *106*, 103705.
(52) Soci, C.; Zhang, A.; Bao, X.-Y.; Kim, H.; Lo, Y.; Wang, D. Nanowire Photodetectors. *J. Nanosci. Nanotechnol.* **2010**, *10*, 1430−1449.
(53) Konstantatos, G.; Sargent, E. H. Nanostructured Materials for Photon Detection. *Nat. Nanotechnol.* **2010**, *5*, 391−400.
(54) Sze, S. M.; Ng, K. K. *Physics of Semiconductor Devices*, 3rd ed.; Wiley-Interscience: Hoboken, N.J., 2007.
(55) Blatter, G.; Greuter, F. Carrier Transport Through Grain Boundaries in Semiconductors. *Phys. Rev. B* **1986**, *33*, 3952.
(56) Greuter, F.; Blatter, G. Electrical Properties of Grain Boundaries in Polycrystalline Compound Semiconductors. *Semicond. Sci. Technol.* **1990**, *5*, 111.
(57) Kovtyukhova, N. I.; Kelley, B. K.; Mallouk, T. E. Coaxially Gated In-Wire Thin-Film Transistors Made by Template Assembly. *J. Am. Chem. Soc.* **2004**, *126*, 12738−12739.
(58) Skinner, K.; Dwyer, C.; Washburn, S. Quantitative Analysis of Individual Metal-CdSe-Metal Nanowire Field-Effect Transistors. *Appl. Phys. Lett.* **2008**, *92*, 112105−112105.
(59) Ayvazian, T.; Xing, W.; Yan, W.; Penner, R. M. Field-Effect Transistors from Lithographically Patterned Cadmium Selenide Nanowire Arrays. *ACS Appl. Mater. Interface* **2012**, *4*, 4445−4452.
(60) Kamins, T. Hall Mobility in Chemically Deposited Polycrystalline Silicon. *J. Appl. Phys.* **1971**, *42*, 4357−4365.
(61) Baccarani, G.; Ricco, B.; Spadini, G. Transport Properties of Polycrystalline Silicon Films. *J. Appl. Phys.* **1978**, *49*, 5565.
(62) Sen, K.; Srivastava, R. S.; Joshi, D. P.; Goyal, V. K. Mobility and its Effect on the Performance of Polycrystalline Solar Cells. *Phys. Status Solidi A* **1983**, *75*, 657−661.
(63) Malta, D.; Von Windheim, J.; Wynands, H.; Fox, B. Comparison of the Electrical Properties of Simultaneously Deposited Homoepitaxial and Polycrystalline Diamond Films. *J. Appl. Phys.* **1995**, *77*, 1536−1545.
(64) Baban, C.; Caraman, M.; Rusu, G. I. Electronic Transport and Photoconductivity of Polycrystalline CdSe Thin Films. *J. Optoelectron. Adv. Mater.* **2006**, *8*, 917−921.
(65) Enache-Pommer, E.; Boercker, J. E.; Aydil, E. S. Electron Transport and Recombination in Polycrystalline TiO Nanowire Dye-Sensitized Solar Cells. *Appl. Phys. Lett.* **2007**, *91*, 123116.
(66) Ghosh, A. K.; Fishman, C.; Feng, T. Theory of the Electrical and Photovoltaic Properties of Polycrystalline Silicon. *J. Appl. Phys.* **2008**, *51*, 446−454.
(67) Peng, K.; Xu, Y.; Wu, Y.; Yan, Y.; Lee, S.-T.; Zhu, J. Aligned Single-Crystalline Si Nanowire Arrays for Photovoltaic Applications. *Small* **2005**, *1*, 1062−1067.
(68) Bour, D.; Nickel, N.; Van de Walle, C.; Kneissl, M.; Krusor, B.; Mei, P.; Johnson, N. Polycrystalline Nitride Semiconductor Light-Emitting Diodes Fabricated on Quartz Substrates. *Appl. Phys. Lett.* **2000**, *76*, 2182−2184.
(69) Petritz, R. L. Theory of Photoconductivity in Semiconductor Films. *Phys. Rev.* **1956**, *104*, 1508.
(70) Rosencher, E.; Vinter, B. *Optoelectronics*; Cambridge University Press: Cambridge, UK, 2002.
(71) Vaitkus, J.; Tomašūnas, R.; Kutra, J.; Petrauskas, M.; Rimkūnas, R.; Žindulis, A. Picosecond Photoconductivity of CdSe and CdTe Thin Films. *J. Cryst. Growth* **1990**, *101*, 826−827.
(72) Capon, J.; Baets, J. D.; Rycke, I. D.; Smet, H. D.; Doutreloigne, J.; Calster, A. V.; Vanfleteren, J. A Lensless Contact-Type Image Sensor Based on a CdSe Photoconductive Array. *Sens. Actuators, A* **1993**, *37*−*38*, 546−551.
(73) Capon, J.; Baets, J. D.; Cubber, A. M. D.; Smet, H. D.; Calster, A. V.; Vanfleteren, J. Analysis of Transient Photoconductivity in CdSe: Cu: Cl Thin Films. *Phys. Status Solidi A* **1994**, *142*, 127−140.
(74) Hu, J.; Odom, T.; Lieber, C. Chemistry and Physics in One Dimension: Synthesis and Properties of Nanowires and Nanotubes. *Acc. Chem. Res.* **1999**, *32*, 435−446.
(75) Duan, X.; Lieber, C. M. General Synthesis of Compound Semiconductor Nanowires. *Adv. Mater.* **2000**, *12*, 298−302.
(76) Cui, Y.; Lauhon, L. J.; Gudiksen, M. S.; Wang, J.; Lieber, C. M. Diameter-Controlled Synthesis of Single-Crystal Silicon Nanowires. *Appl. Phys. Lett.* **2001**, *78*, 2214−2216.
(77) Fanfair, D. D.; Korgel, B. A. Bismuth Nanocrystal-Seeded III-V Semiconductor Nanowire Synthesis. *Cryst. Growth Des.* **2005**, *5*, 1971−1976.
(78) Lu, X.; Fanfair, D. D.; Johnston, K. P.; Korgel, B. A. High Yield Solution-Liquid-Solid Synthesis of Germanium Nanowires. *J. Am. Chem. Soc.* **2005**, *127*, 15718−15719.
(79) Jeong, U.; Xia, Y.; Yin, Y. Large-Scale Synthesis of Single-Crystal CdSe Nanowires Through a Cation-Exchange Route. *Chem. Phys. Lett.* **2005**, *416*, 246−250.
(80) Lee, D. C.; Hanrath, T.; Korgel, B. A. The Role of Precursor-Decomposition Kinetics in Silicon-Nanowire Synthesis in Organic Solvents. *Angew. Chem., Int. Ed.* **2005**, *44*, 3573−3577.
(81) Wang, G.; Park, M.; Liu, H.; Wexler, D.; Chen, J. Synthesis and Characterization of One-Dimensional CdSe Nanostructures. *Appl. Phys. Lett.* **2006**, *88*, 193115 (3 pp).
(82) Liu, C.; Wu, P.; Sun, T.; Dai, L.; Ye, Y.; Ma, R.; Qin, G. Synthesis of High Quality n-type CdSe Nanobelts and Their Applications in Nanodevices. *J. Phys. Chem. C* **2009**, *113*, 14478−14481.
(83) Takahashi, T.; Takei, K.; Ho, J. C.; Chueh, Y.-L.; Fan, Z.; Javey, A. Monolayer Resist for Patterned Contact Printing of Aligned Nanowire Arrays. *J. Am. Chem. Soc.* **2009**, *131*, 2102−2103.
(84) Yerushalmi, R.; Jacobson, Z. A.; Ho, J. C.; Fan, Z.; Javey, A. Large Scale, Highly Ordered Assembly of Nanowire Parallel Arrays by Differential Roll Printing. *Appl. Phys. Lett.* **2007**, *91*, 203104 (3 pp).
(85) Fan, Z.; Ho, J. C.; Jacobson, Z. A.; Yerushalmi, R.; Alley, R. L.; Razavi, H.; Javey, A. Wafer-Scale Assembly of Highly Ordered Semiconductor Nanowire Arrays by Contact Printing. *Nano Lett.* **2008**, *8*, 20−25.
(86) Fan, Z.; Ho, J. C.; Jacobson, Z. A.; Razavi, H.; Javey, A. Large-Scale, Heterogeneous Integration of Nanowire Arrays for Image Sensor Circuitry. *Proc. Natl. Acad. Sci. U.S.A.* **2008**, *105*, 11066−11070.
(87) Melosh, N. A.; Boukai, A.; Diana, F.; Gerardot, B.; Badolato, A.; Petroff, P. M.; Heath, J. R. Ultrahigh-Density Nanowire Lattices and Circuits. *Science* **2003**, *300*, 112−115.
(88) Huang, J.; Fan, R.; Connor, S.; Yang, P. One-Step Patterning of Aligned Nanowire Arrays by Programmed Dip Coating. *Angew. Chem., Int. Ed.* **2007**, *119*, 2466−2469.
(89) Yaman, M.; Khudiyev, T.; Ozgur, E.; Kanik, M.; Aktas, O.; Ozgur, E. O.; Deniz, H.; Korkut, E.; Bayindir, M. Arrays of Indefinitely Long Uniform Nanowires and Nanotubes. *Nat. Mater.* **2011**, *10*, 494−501.
(90) Ozgur, E.; Aktas, O.; Kanik, M.; Yaman, M.; Bayindir, M. Macroscopic Assembly of Indefinitely Long and Parallel Nanowires into Large Area Photodetection Circuitry. *Nano Lett.* **2012**, *12*, 2483−2487.
(91) Ayvazian, T.; van der Veer, W. E.; Xing, W.; Yan, W.; Penner, R. M. Electroluminescent, Polycrystalline Cadmium Selenide Nanowire Arrays. *ACS Nano* **2013**, *7*, 9469−9479.
(92) Menke, E. J.; Thompson, M. A.; Xiang, C.; Yang, L. C.; Penner, R. M. Lithographically Patterned Nanowire Electrodeposition. *Nat. Mater.* **2006**, *5*, 914−919.
(93) Xiang, C.; Kung, S.-C.; Taggart, D. K.; Yang, F.; Thompson, M. A.; Gueell, A. G.; Yang, Y.; Penner, R. M. Lithographically Patterned Nanowire Electrodeposition: A Method for Patterning Electrically Continuous Metal Nanowires on Dielectrics. *ACS Nano* **2008**, *2*, 1939−1949.
(94) Xiang, C.; Yang, Y.; Penner, R. M. Cheating the Diffraction Limit: Electrodeposited Nanowires Patterned by Photolithography. *Chem. Commun.* **2009**, 859−873.
(95) Kung, S.-C.; van der Veer, W. E.; Yang, F.; Donavan, K. C.; Penner, R. M. 20 μs Photocurrent Response from Lithographically Patterned Nanocrystalline Cadmium Selenide Nanowires. *Nano Lett.* **2010**, *10*, 1481−1485.
(96) Kung, S.-C.; Xing, W.; van der Veer, W. E.; Yang, F.; Donavan, K. C.; Cheng, M.; Hemminger, J. C.; Penner, R. M. Tunable Photoconduction Sensitivity and Bandwidth for Lithographically Patterned

Nanocrystalline Cadmium Selenide Nanowires. *ACS Nano* **2011**, *5*, 7627−7639.
(97) Xing, W.; Yan, W.; Ayvazian, T.; Wang, Y.; Potma, E. O.; Penner, R. M. Electrodeposited Light-Emitting Nanojunctions. *Chem. Mater.* **2013**, *25*, 623−631.
(98) Xing, W.; Kung, S.-C.; van der Veer, W. E.; Yan, W.; Ayvazian, T.; Kim, J. Y.; Penner, R. M. High-Throughput Fabrication of Photoconductors with High Detectivity, Photosensitivity, and Bandwidth. *ACS Nano* **2012**, *6*, 5627−5634.
(99) Li, Q.; Brown, M.; Hemminger, J.; Penner, R. Luminescent Polycrystalline Cadmium Selenide Nanowires Synthesized by Cyclic Electrodeposition/Stripping Coupled with Step Edge Decoration. *Chem. Mater.* **2006**, *18*, 3432−3441.
(100) Li, Q.; Penner, R. M. Photoconductive Cadmium Sulfide Hemicylindrical Shell Nanowire Ensembles. *Nano Lett.* **2005**, *5*, 1720−1725.
(101) Pena, D. J.; Mbindyo, J. K.; Carado, A. J.; Mallouk, T. E.; Keating, C. D.; Razavi, B.; Mayer, T. S. Template Growth of Photoconductive Metal-CdSe-Metal Nanowires. *J. Phys. Chem. B* **2002**, *106*, 7458−7462.
(102) Gu, X. W.; Shadmi, N.; Yarden, T. S.; Cohen, H.; Joselevich, E. Photoconductive CdSe Nanowire Arrays, Serpentines, and Loops Formed by Electrodeposition on Self-Organized Carbon Nanotubes. *J. Phys. Chem. C* **2012**, *116*, 20121−20126.
(103) He, Z.; Jie, J.; Zhang, W.; Zhang, W.; Luo, L.; Fan, X.; Yuan, G.; Bello, I.; Lee, S.-T. Tuning Electrical and Photoelectrical Properties of CdSe Nanowires via Indium Doping. *Small* **2009**, *5*, 345−350.
(104) He, Z.; Zhang, W.; Zhang, W.; Jie, J.; Luo, L.; Yuan, G.; Wang, J.; Wu, C. M. L.; Bello, I.; Lee, C.-S. High-Performance CdSe:In Nanowire Field-Effect Transistors Based on Top-Gate Configuration with High-k Non-Oxide Dielectrics. *J. Phys. Chem. C* **2010**, *114*, 4663−4668.
(105) Jie, J. S.; Zhang, W. J.; Jiang, Y.; Lee, S. T. Single-Crystal CdSe Nanoribbon Field-Effect Transistors and Photoelectric Applications. *Appl. Phys. Lett.* **2006**, *89*, 133118 (3pp).
(106) Yan, Y.; Liao, Z.-M.; Bie, Y.-Q.; Wu, H.-C.; Zhou, Y.-B.; Fu, X.-W.; Yu, D.-P. Luminescence Blue-Shift of CdSe Nanowires Beyond the Quantum Confinement Regime. *Appl. Phys. Lett.* **2011**, *99*, 103103 (3 pp).
(107) Calster, A. V.; Vanfleteren, J.; Rycke, I. D.; Baets, J. D. On the Field Effect in Polycrystalline CdSe Thin-Film Transistors. *J. Appl. Phys.* **1988**, *64*, 3282−3286.
(108) Birkmire, R. W.; Eser, E. Polycrystalline Thin Film Solar Cells: Present Status and Future Potential. *Annu. Rev. Mater. Sci.* **1997**, *27*, 625−653.
(109) Benamar, E.; Rami, M.; Fahoume, M.; Chraibi, F.; Ennaoui, A. Electrodeposited Cadmium Selenide Films for Solar Cells. *Ann. Chim.-Sci. Mater.* **1998**, *23*, 369−372.
(110) Lee, K.-S.; Kim, I.; Gullapalli, S.; Wong, M. S.; Jabbour, G. E. Enhanced Performance of Hybrid Solar Cells using Longer Arms of Quantum Cadmium Selenide Tetrapods. *Appl. Phys. Lett.* **2011**, *99*, 223515 (3 pp).
(111) Alamgir, K.; Pervaiz, T.; Arif, S. Characterization of Cadmium Selenide Thin Film for Solar Cell Application. *Energy Sources, Part A* **2012**, *34*, 297−305.
(112) Oertel, D. C.; Bawendi, M. G.; Arango, A. C.; Bulovic, V. Photodetectors Based on Treated CdSe Quantum-Dot Films. *Appl. Phys. Lett.* **2005**, *87*, 213505 (3 pp).
(113) Jiang, Y.; Zhang, W. J.; Jie, J. S.; Meng, X. M.; Fan, X.; Lee, S.-T. Photoresponse Properties of CdSe Single-Nanoribbon Photodetectors. *Adv. Funct. Mater.* **2007**, *17*, 1795−1800.
(114) Singh, A.; Li, X.; Protasenko, V.; Galantai, G.; Kuno, M.; Xing, H. G.; Jena, D. Polarization-Sensitive Nanowire Photodetectors Based on Solution-Synthesized CdSe Quantum-Wire Solids. *Nano Lett.* **2007**, *7*, 2999−3006.
(115) Klein, J.; Herrick, R.; Palmer, D.; Sailor, M.; Brumlik, C.; Martin, C. Electrochemical Fabrication of Cadmium Chalcogenide MicrodiodeI Arrays. *Chem. Mater.* **1993**, *5*, 902−904.
(116) Schierhorn, M.; Boettcher, S. W.; Ivanovskaya, A.; Norvell, E.; Sherman, J. B.; Stucky, G. D.; Moskovits, M. Fabrication and Electrochemical Photovoltaic Response of CdSe Nanorod Arrays. *J. Phys. Chem. C* **2008**, *112*, 8516−8520.
(117) Kressin, A.; Doan, V.; Klein, J.; Sailor, M. Synthesis of Stoichiometric Cadmium Selenide Films via Sequential Monolayer Electrodeposition. *Chem. Mater.* **1991**, *3*, 1015−1020.
(118) Brown, M. A.; Hemminger, J. C.; Penner, R. M. Luminescent Polycrystalline Cadmium Selenide Nanowires Synthesized by Cyclic Electrodeposition/Stripping Coupled with Step Edge Decoration. *Chem. Mater.* **2006**, *18*, 3432−3441.
(119) Patterson, A. The Scherrer Formula for X-ray Particle Size Determination. *Phys. Rev.* **1939**, *56*, 978−982.
(120) Zach, M.; Ng, K.; Penner, R. Electrochemical Step Edge Decoration. *Science* **2000**, *290*, 2120−2123.
(121) Penner, R. M. Mesoscopic Metal Particles and Wires by Electrodeposition. *J. Phys. Chem. B* **2002**, *106*, 3339−3353.
(122) Walter, E.; Murray, B.; Favier, F.; Kaltenpoth, G.; Grunze, M.; Penner, R. Noble and Coinage Metal Nanowires by Electrochemical Step Edge Decoration. *J. Phys. Chem. B* **2002**, *106*, 11407−11411.
(123) Penner, R. M. In *Modern Aspects of Electrochemistry*; White, R. E.; Springer: New York, 2009; Vol. *45*, pp 175−206.
(124) Peyser, L.; Lee, T.; Dickson, R. Mechanism of Ag-n Nanocluster Photoproduction from Silver Oxide Films. *J. Phys. Chem. B* **2002**, *106*, 7725−7728.
(125) Lee, T.; Gonzalez, J.; Dickson, R. Strongly Enhanced Field-Dependent Single-Molecule Electrolurninescence. *Proc. Natl. Acad. Sci. U.S.A.* **2002**, *99*, 10272−10275.
(126) Lee, T.; Dickson, R. Single-Molecule LEDs From Nanoscale Electroluminescent Junctions. *J. Phys. Chem. B* **2003**, *107*, 7387−7390.
(127) Maekinen, A. J.; Foos, E. E.; Wilkinson, J.; Long, J. P. STM-Induced Light Emission From Substrate-Tethered Quantum Dots. *J. Phys. Chem. C* **2007**, *111*, 8188−8194.
(128) Dorn, A.; Huang, H.; Bawendi, M. G. Electroluminescence from Nanocrystals in an Electromigrated Gap Composed of Two Different Metals. *Nano Lett.* **2008**, *8*, 1347−1351 , PMID: 18393538.
(129) Hoshino, K.; Rozanski, L. J.; Bout, D. A. V.; Zhang, X. Direct Fabrication of Nanoscale Light Emitting Diode on Silicon Probe Tip for Scanning Microscopy. *J. Microelectromech. Syst.* **2008**, *17*, 4−10.
(130) Khanna, S. K.; Lambe, J. Inelastic Electron Tunneling Spectroscopy. *Science* **1983**, *220*, 1345−1351.
(131) Qiu, X.; Nazin, G.; Ho, W. Vibrationally Resolved Fluorescence Excited with Submolecular Precision. *Science* **2003**, *299*, 542−546.
(132) Kim, J.; Benson, O.; Kan, H.; Yamamoto, Y. A Single-Photon Turnstile Device. *Nature* **1999**, *397*, 500−503.
(133) Simmons, J. Poole-Frenkel Effect and Schottky Effect in Metal-Insulator-Metal Systems. *Phys. Rev.* **1967**, *155*, 657.
(134) Simmons, J. Conduction in Thin Dielectric Films. *J. Phys. D: Appl. Phys.* **1971**, *4*, 613−657.
(135) Schubert, E. *Light-Emitting Diodes*, 2nd ed.; Cambridge Unversity Press: Cambridge, UK, 2006.
(136) Sato, M.; Kawai, S.; Yamada, F. Heat Treatment of CdSe Thin Films and Application to Photopotentiometers. *Electrocomponent Sci. Technol.* **1981**, *8*, 199−206.
(137) Raturi, A.; Thangaraj, R.; Ram, P.; Tripathi, B.; Agnihotri, O. Non-Equilibrium Carrier Relaxation in Sprayed CdSe Films. *Thin Solid Films* **1983**, *106*, 257−261.
(138) Garcia, V. M.; Nair, M. T. S.; Nair, P. K.; Zingaro, R. A. Preparation of Highly Photosensitive CdSe Thin Films by a Chemical Bath Deposition Technique. *Semicond. Sci. Technol.* **1996**, *11*, 427−432.
(139) Gao, T.; Li, Q.; Wang, T. CdS Nanobelts as Photoconductors. *Appl. Phys. Lett.* **2005**, *86*, 173105−173105.
(140) Ye, Y.; Dai, L.; Wen, X.; Wu, P.; Pen, R.; Qin, G. High-Performance Single CdS Nanobelt Metal-Semiconductor Field-Effect Transistor-Based Photodetectors. *ACS Appl. Mater. Interface* **2010**, *2*, 2724−2727.
(141) Wang, X.; Wang, J.; Zhou, M.; Zhu, H.; Wang, H.; Cui, X.; Xiao, X.; Li, Q. CdTe Nanorod Arrays on ITO: From Microstructure to Photoelectrical Property. *J. Phys. Chem. C* **2009**, *113*, 16951−16953.

(142) Pourret, A.; Guyot-Sionnest, P.; Elam, J. W. Atomic Layer Deposition of ZnO in Quantum Dot Thin Films. *Adv. Mater.* **2009**, *21*, 232−235.
(143) Hegg, M. C.; Horning, M. P.; Baehr-Jones, T.; Hochberg, M.; Lin, L. Y. Nanogap Quantum Dot Photodetectors with High Sensitivity and Bandwidth. *Appl. Phys. Lett.* **2010**, *96*, 101118.
(144) Wu, P.; Dai, Y.; Sun, T.; Ye, Y.; Meng, H.; Fang, X.; Yu, B.; Dai, L. Impurity-Dependent Photoresponse Properties in Single CdSe Nanobelt Photodetectors. *ACS Appl. Mater. Interface* **2011**, *3*, 1859−1864.
(145) Gudiksen, M.; Lauhon, L.; Wang, J.; Smith, D.; Lieber, C. Growth of Nanowire Superlattice Structures for Nanoscale Photonics and Electronics. *Nature* **2002**, *415*, 617−620.